JOURNAL OF APPLIED ELECTROCHEMISTRY 10 (1980) 611–621

# *The influence of temperature on the current peak multiplicity related to the nickel hydroxide electrode*

H. GÓMEZ MEIER, J. R. VILCHE, A. J. ARVIA

*Instituto de Investigaciones Fisicoquimicas Teóricas y Aplicadas, División Electroquimica, Sucursal 4 - Casilla de Correo 16, 1900 La Plata, Argentina*

Received 15 October 1979

The splitting of the anodic and cathodic potentiodynamic *E/I* display of the nickel hydroxide electrode in 1 N KOH between 0 and 75° C is reported. The formal first order rate constants for the chemical reactions which occur simultaneously with the electrochemical steps, and the corresponding activation energies are evaluated. The results are discussed on the basis of the reaction model recently proposed for the nickel hydroxide electrode.

## 1. Introduction

The potentiodynamic *E/I* displays of Ni/KOH(aq) interfaces run with complex perturbations in the potential range associated with the nickel hydroxide electrode reactions [$Ni(OH)_2 = NiOOH + H^+ + e$] exhibit a multiplicity of anodic and cathodic current peaks [1–8]. The relative contribution of the different current peaks in the electrochemical spectrum obtained through a triangular potential sweep technique is sensitive to the characteristics of the potential perturbation programme. The gradual changes of the electrochemical spectra produced through the systematic variation of the perturbation parameters reveal the existence of non-equilibrium species related to the $Ni(OH)_2$ and the NiOOH species. The rates of the transformations between the various species can be estimated when the type of potentiodynamic perturbations described for the study of film ageings are used [9]. The reactions may involve rearrangement of the water of hydration in the film species or a change of defect concentration in the hydrated species. The relative concentration of the different species related to each oxidation state of nickel is modified during ageing, hence so is the overpotential required for the corresponding electrochemical reaction. Therefore, the phenomenological description of the overall nickel hydroxide electrode reaction should comprise electron transfer stages as well as simultaneous chemical reactions involving the various solid film species.

The present paper reports the change in distribution of the multiple current peaks, both anodic and cathodic, observed during the potentiodynamic perturbations of the Ni/KOH(aq) interface under a relatively wide range of perturbation conditions, in the 0 to 75° C range. For this purpose the electrochemical interface is subjected to the sequence of triangular potential perturbations required to produce the potentiodynamic ageing of the electrochemically formed films. Besides confirming the presence of various non-equilibrium $Ni(OH)_2$ and NiOOH species at the nickel hydroxide electrodes, the present results furnish additional data related to the energetics of the chemical reactions coupled to the corresponding electrochemical processes according to the reaction scheme recently postulated [7, 8].

## 2. Experimental

The experimental set-up was the same as that already described in previous publications [5–8, 10, 11]. Specpure (Johnson, Matthey and Co. Ltd) nickel wires (0.5 mm diameter, 0.25 $cm^2$) were used as the working electrodes in nitrogen saturated 1 N KOH solution at 0, 25, 50 and 75° C. The solution was prepared from thrice distilled water and analytical grade (p.a. Merck) reagents. Potentials were measured versus a

0021–891X/80/050611–11$03.10/0  

saturated calomel electrode but in the text they are referred to the standard hydrogen electrode scale.

Two types of $E/I$ profiles are presented:

(a) $E/I$ displays resulting from the application of conventional repetitive triangular potential sweeps, to determine the number of cycles required to attain the stabilized $E/I$ display; and

(b) the $E/I$ displays resulting from the application of the potentiodynamic-ageing perturbation technique, to evaluate the current peak multiplicity of the potentiodynamic $E/I$ profiles related to the nickel hydroxide electrode reactions.

The latter involves the potential perturbation programmes depicted in Fig. 1. Accordingly, the electrochemical interface was perturbed with the following sequence of potentiodynamic sweeps. (a) Repetitive triangular potential sweeps (RTPS) run at a preset potential sweep rate ($v$) between the cathodic ($E_{s,c}$) and anodic ($E_{s,a}$) switching potentials until a reproducible $E/I$ contour was attained. The reproducible $E/I$ contour is identified with the number '1'. The potential sweep rate was changed in the $0.1\ V\ s^{-1} \leqslant v \leqslant 0.3\ V\ s^{-1}$ range. The $E_{s,c}$ and $E_{s,a}$ values were conveniently adjusted at each temperature to cover the whole potential range related to the nickel hydroxide electrode reactions. (b) Immediately afterwards, a sequence of intermediate triangular potential sweeps covering a smaller potential amplitude (indicated by 1') was applied during the time $\tau$. The corresponding switching potentials either $E'_{s,c}$ (Fig. 1a) or $E'_{s,a}$ (Fig. 1b) within the potential range between $E_{s,a}$ and $E_{s,c}$, were adjusted according to the kinetic characteristics of the process. The time $\tau$ was changed within the $1\ min \leqslant \tau \leqslant 15\ min$ range. (c) Finally, immediately after the intermediate potential perturbation a single potential sweep was run from $E_{s,a}$ towards $E_{s,c}$ or vice versa. The latter potential sweep revealed the ageing effects through the shift of the current peaks and their splitting into multiple current peaks. The final $E/I$ single sweeps are identified in the figures with the numbers 2, 3, 4, etc., each one corresponding to a particular time $\tau$. Further details of the experimental techniques are described in previous publications [5–7, 10].

## 3. Results

### 3.1. *The stabilized E/I profile*

The sequence of $E/I$ profiles resulting from RTPS in the potential range of the $Ni(OH)_2$ electrode at $0.1\ V\ s^{-1}$ initiated from $E_{s,c}$ [10, 11], changes gradually from the first potential sweep (Figs. 2 and 3) to attain the stabilized $E/I$ profile. At 0° C, the first positive potential-going sweep exhibits no anodic current peak, but the returning negative potential-going scan presents a clear cathodic

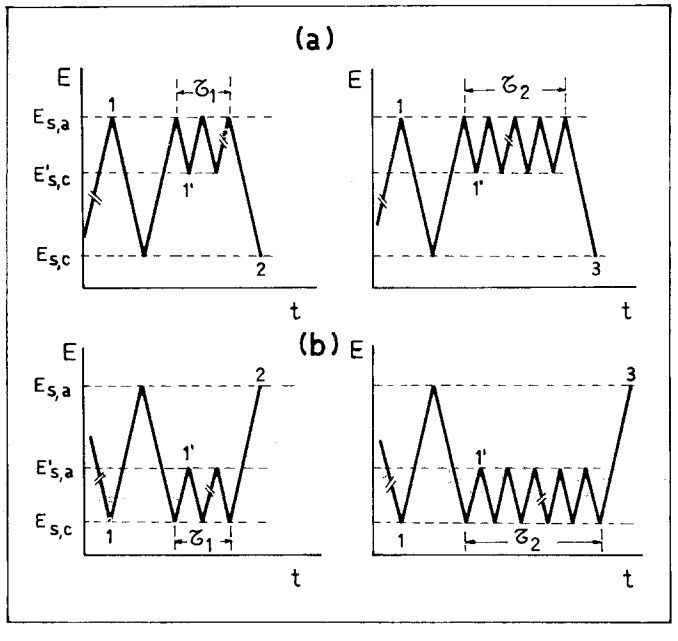


Fig. 1. Potential–time perturbation programmes for the potentiodynamic ageing experiments. The numbers on the potential–time programmes correspond to those included in Figs. 5–8. (a) Corresponds to the potentiodynamic ageing of the cathodic reaction products; (b) corresponds to the potentiodynamic ageing of the anodic reaction products.

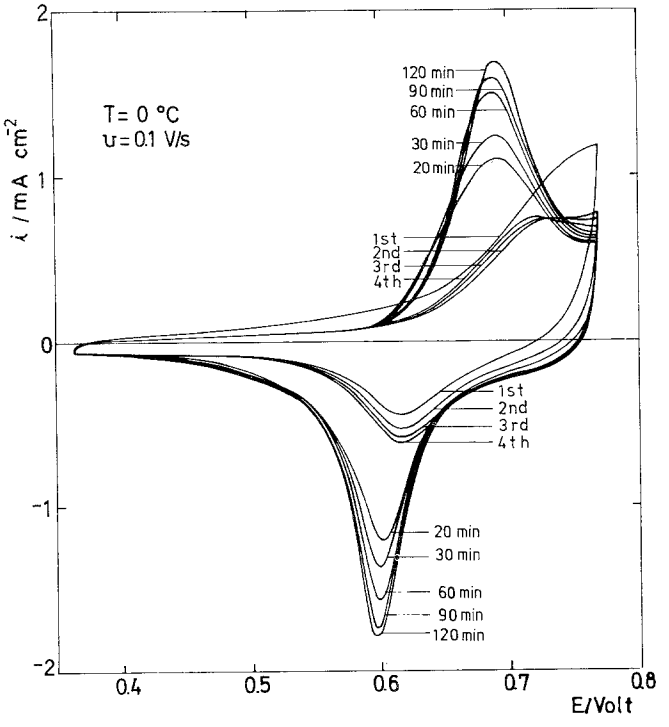


Fig. 2. Gradual change of the $E/I$ profile under RTPS at $v = 0.1\ \mathrm{V\,s^{-1}}$; 0° C. The $E/I$ displays are shown for the first, second, third and fourth sweeps together with those recorded after different times of RTPS.

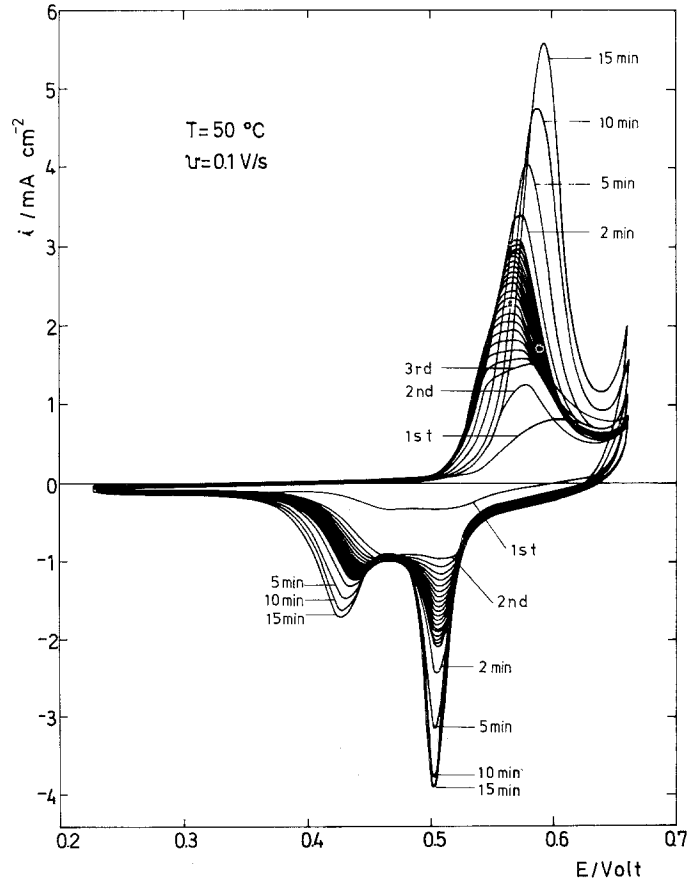


Fig. 3. Gradual change of the $E/I$ under RTPS at $v = 0.1\ \mathrm{V\,s^{-1}}$; 50° C. The $E/I$ displays are shown for the first, second and third sweeps together with those recorded after different times of RTPS.

current peak. The anodic current peak which during the third potential sweep is recorded at about 0.73 V, increases in height on continuing the potential cycling and simultaneously its peak potential shifts towards more negative values, reaching about 0.69 V after 60 min potential cycling. Afterwards the peak potential moves slightly backwards to more positive values. This effect is more evident at 50° C, but the current peaks both anodic and cathodic are displayed within narrower potential ranges as the temperature increases.

Under comparable perturbation conditions, the number of cycles to attain the stabilized RTPS $E/I$ contour decreases as the temperature increases. Thus, at 0° C, the stable $E/I$ contour is reached after 2.5 h cycling at 0.1 V $s^{-1}$ in the 0.44 to 0.84 V range. At low temperatures the stabilized $E/I$ profile shows on the positive-going potential excursion a single broad and somewhat symmetric anodic current peak in the potential range preceding the oxygen evolution and during the negative-going potential excursion a single cathodic current peak with similar characteristics. At the highest temperatures there is also a single anodic current peak in the stabilized RTPS $E/I$ profile although it becomes narrower than that recorded at low temperatures; the corresponding cathodic current peak is now definitely split into two current peaks. The cathodic current peak located at more positive potentials is thinner but higher than that located at more negative potentials. The latter, at 25° C, appears as a shoulder in the $E/I$ display [5–7].

Once the stabilized RTPS $E/I$ profile is attained, the anodic to cathodic charge ratio ($Q_a/Q_c$) is, within experimental error, equal to one. Within the potential range covering the complete nickel hydroxide electrode reactions either the $Q_a$ or the $Q_c$ maximum charge associated with the stabilized RTPS $E/I$ profiles run at 0.1 V $s^{-1}$ is 1.7 mC $cm^{-2}$. This charge value is independent of the temperature but decreases with the potential sweep rate as reported earlier [6].

The potentials of the current peaks in the stabilized RTPS $E/I$ profile decrease as the temperature increases according to a linear $E_p$ versus $T$ plot (Fig. 4). The temperature coefficient of the corresponding electrochemical reactions is in the order of $-2$ mV $K^{-1}$. This figure is within

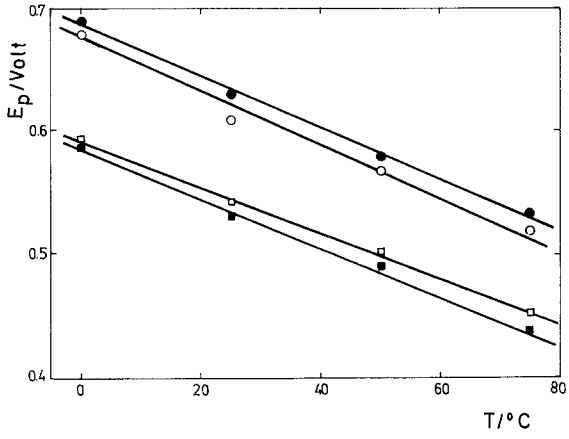


Fig. 4. The dependence of peak potentials on temperature. (●) and (■) correspond respectively to the main anodic and cathodic current peaks obtained with RTPS. (○) and (□) correspond to the potentials of current peaks I and III recorded after comparable potentiodynamic ageings. The $(\Delta E_p/\Delta T)_T$ ratios measured are $-2.1$, $-2.0$, $-2.2$ and $-1.8$ mV $K^{-1}$, respectively.

the order of magnitude of the isothermal temperature coefficient of electrode reactions involving hydroxide species [12].

### 3.2. *The splitting of the anodic current peak*

To produce the splitting of the anodic current peak $E_{s,a}$, $E_{s,c}$, $v$, $E'_{s,a}$ and $\tau$ are systematically changed (Figs. 5 and 6). Thus, at 0° C, the potentiodynamic $E/I$ display run immediately after the potentiodynamic ageing presents two anodic current peaks located at about 0.68 V and 0.72 V, respectively, instead of the former single anodic current peak at 0.7 V. At 75° C, the single anodic current peak at 0.52 V divides into two anodic current peaks, one at about 0.51 V and another at about 0.55 V. The separation of the two anodic current peaks approaches 0.05 V at any temperature within the 0 to 75° C range as $\tau$ increases. In all cases, the total anodic charge appearing in the $E/I$ display run immediately after the potentiodynamic ageing is equal to the charge corresponding to the stabilized RTPS $E/I$ display, independent of the extent of splitting of the anodic current peak.

Under comparable conditions, the time required to reach the same extent of the anodic current peak splitting decreases remarkably as the temperature increases. The best definition of the

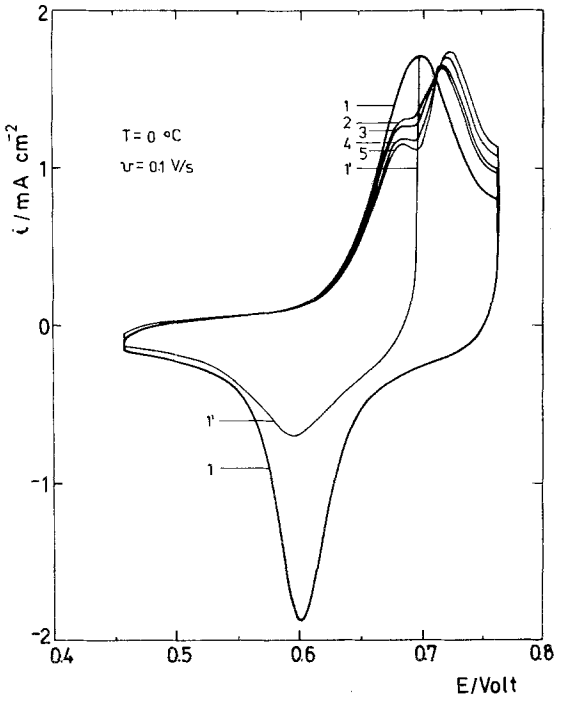


Fig. 5. Potentiodynamic $E/I$ displays obtained with perturbation programme (b) with a constant $E'_{s,a}$ and different $\tau$, at 0° C. $\tau_1 = 2$ min (2); $\tau_2 = 5$ min (3); $\tau_3 = 10$ min (4) and $\tau_4 = 15$ min (5).

anodic current peak components is established at the lowest temperature because of the relatively small overlap of the $E/I$ profiles related to the nickel hydroxide electrode reaction and to the oxygen evolution reaction.

The $E/I$ profiles obtained after potentiodynamic ageing at different times $\tau$ exhibit a crossing potential, $E_{cc}$. The values of $E_{cc}$ decrease as the temperature increases, following approximately the same temperature dependence as that observed for the anodic current peak of the stabilized RTPS $E/I$ profile (Fig. 4). Tentatively, the $E_{cc}$ values can be interpreted as equivalent to the isobiestic point observed in charge transfer complex spectra [13]. The gradual changes of the successive intermediate RTPS $E/I$ displays run between $E'_{s,c}$ and $E_{s,a}$ are comparable to those already described for the RTPS $E/I$ profiles depicted in Figs. 2 and 3.

### 3.3. *The splitting of the cathodic current peak*

The splitting of the cathodic current peak occurs similarly to that of the anodic current peak. The overall charge of the cathodic current peak after the splitting remains practically constant, but the phenomenology of the splitting process (Figs. 7 and 8) now appears rather more involved than that described for the anodic current peak. The relative contribution of the current peaks and humps generated by the splitting of the cathodic current peak changes considerably with the temperature. Thus, at 0° C the stabilized cathodic current peak recorded at 0.58 V after the potentiodynamic ageing reveals three contributions, namely a major current peak at about

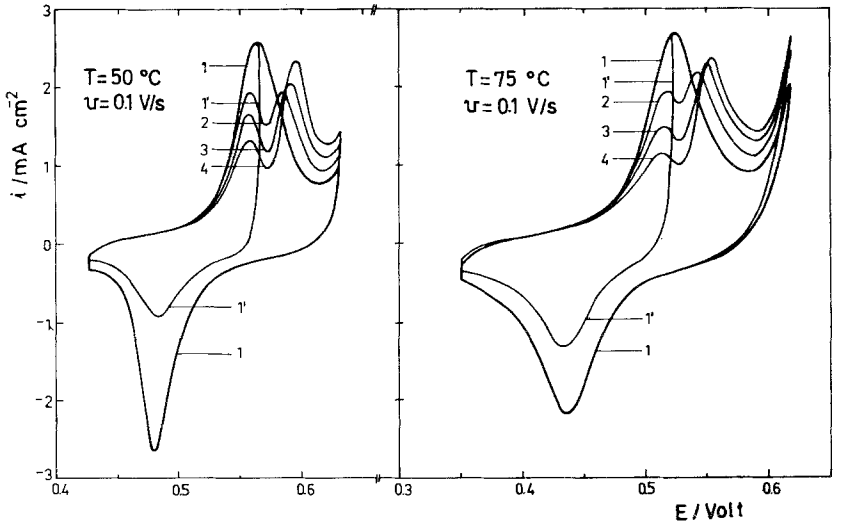


Fig. 6. Potentiodynamic $E/I$ displays obtained with perturbation programme (b) with a constant $E'_{s,a}$ and different $\tau$, at 50° C, $\tau_1 = 1$ min (2); $\tau_2 = 3$ min (3) and $\tau_3 = 5$ min (4). At 75° C; $\tau_1 = 0.5$ (2); $\tau_2 = 1.5$ (3) and $\tau_3 = 3$ min (4).

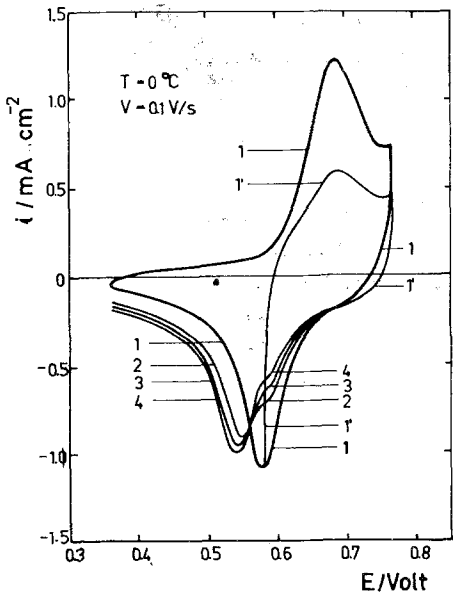


Fig. 7. Potentiodynamic *E/I* displays recorded with perturbation programme (a) at a constant $E'_{s,a}$ and different $\tau$, at 0° C. $\tau_1 = 3$ min (2); $\tau_2 = 6$ min (3) and $\tau_3 = 10$ min (4).

0.54 V, a shoulder at about 0.59 V, a potential which lies within the potential range of the stabilized cathodic current peak potential, and a small shoulder at about 0.45 V, which is hardly distinguishable (Fig. 7). The latter, however, at 25° C [6], defines a net current shoulder but at higher temperatures the *E/I* contour shows a clear current peak which competes in height with that of the major current peak.

At 50° C (Fig. 8) the cathodic current profile splits into three clearly distinguishable current peaks. The distribution of the cathodic current peaks is such that most of the charge involved in the *E/I* display after the potentiodynamic ageing moves towards more negative potentials as the time $\tau$ increases. As with the anodic process, the cathodic current peak splitting should be associated with the occurrence of different reactive species whose relative concentrations are time-dependent.

## 4. Discussion

### 4.1. *The probable reaction mechanism*

The results obtained through the complex potentiodynamic perturbation of the Ni/1 N KOH interface in the 0–75° C range correlate with those previously reported at 25° C. The latter were interpreted through a scheme of squares, involving two electrochemical and two chemical reactions [7]. Otherwise, data derived from the perturbation of the electrochemical interface with triangularly modulated triangular potential sweeps showed that the square reaction model should be extended to include the corresponding crossed reactions [8]. Likewise, the characteristics of the genesis of the stabilized potentiodynamic *E/I* profiles (Figs. 2 and 3) correlates with the assumption of a multiplicity of conjugate redox couples in the potential range of the nickel hydroxide electrode. Thus, the reaction mechanism proposed for the nickel hydroxide electrode was

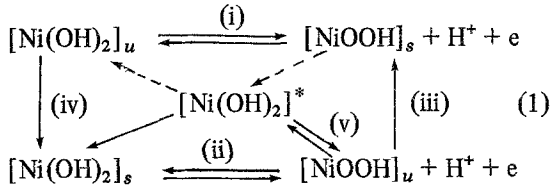


(1)

where the subscripts *s* and *u* denote stable and unstable reacting species respectively and the asterisk indicates an intermediate species associated with the crossed reactions. When the crossed reactions are neglected this reaction model corresponds to the reaction pathway proposed earlier [14] if $[Ni(OH)_2]_u = \alpha$-$Ni(OH)_2$; $[NiOOH]_s = \gamma$-NiOOH; $[Ni(OH)_2]_s = \beta$-$Ni(OH)_2$ and $[NiOOH]_u = \beta$-NiOOH. But these assignments are certainly not fully proven. One way to confirm the scheme, particularly the contribution of chemical reactions, is through the evaluation of the energy terms from the temperature dependences of the kinetic data. Then, the most likely correlation between the already known structural configuration and the *u* and *s* species involved in the reaction mechanism can be established.

### 4.2. *Evaluation of the rate constants of the chemical steps*

The reaction mechanism of the nickel hydroxide electrode in Scheme 1 implies the existence of chemical reactions (iii) and (iv). Reactions (iii) and (iv) are characterized by the rate constants $k_1^0$ and $k_2^0$, respectively. The evaluation of the

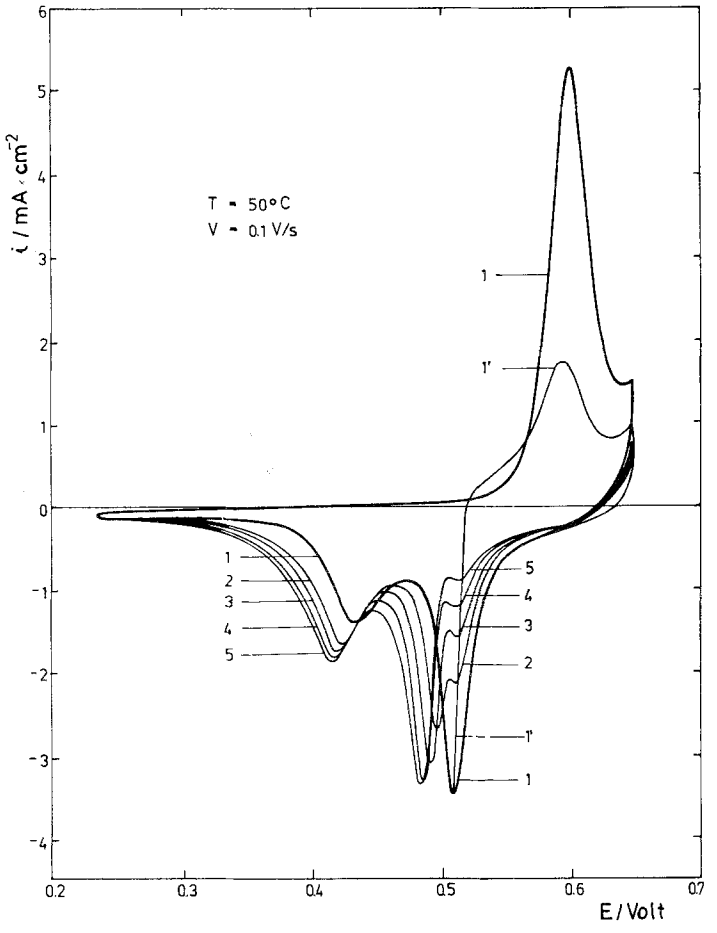


Fig. 8. Potentiodynamic *E/I* displays obtained with perturbation programme (a) at a constant $E'_{s,c}$ and different $\tau$, at 50° C. $\tau_1 = 1$ min (2); $\tau_2 = 3$ min (3); $\tau_3 = 6$ min (4) and $\tau_4 = 10$ min (5).

formal rate constants ($k_1$ and $k_2$) is made following the procedure already applied to the data obtained at 25° C, after assuming that in Scheme 1 the crossed reactions can be neglected [7, 8]. Therefore, the rate of the reaction

$$[Ni(OH)_2]_u \xrightarrow{k_1} [Ni(OH)_2]_s \qquad (2)$$

assisted by the potentiodynamic ageing, can be evaluated through the relative change of the charges involved in the anodic current peaks, assuming that the charge of each anodic current peak represents a single electrochemical reaction. Thus, $Q_I$, the charge of the first anodic current peak component, is associated with the reaction:

$$[Ni(OH)_2]_u \rightleftharpoons [NiOOH]_s + H^+ + e \qquad (3)$$

while $Q_{II}$, the charge of the second anodic current peak component, corresponds to the reaction:

$$[Ni(OH)_2]_s \rightleftharpoons [NiOOH]_u + H^+ + e \qquad (4)$$

Since the overall anodic charge after the correction for the oxygen evolution baseline is $Q_{T,a} = Q_I + Q_{II}$ at any splitting of the anodic current peak, the relative contribution of $Q_I$ and $Q_{II}$ should depend on the duration of the potentiodynamic ageing. The magnitudes of $Q_I$ and $Q_{II}$ are determined from the positive potential-going *E/I* display run immediately after the potentiodynamic ageing applied during time $\tau$. For this purpose a conventional graphical integration and trial and error procedure is used [7]. The error involved in the estimation of $Q_I$ and $Q_{II}$ is less than 5%. The corresponding formal rate constant, $k_1$, for the reaction assisted by the potentiodynamic ageing is evaluated using a first order rate equation:

$$-\frac{dQ_I}{d\tau} = k_1 Q_1 = \frac{dQ_{II}}{d\tau} \qquad (5)$$

which after integration yields:

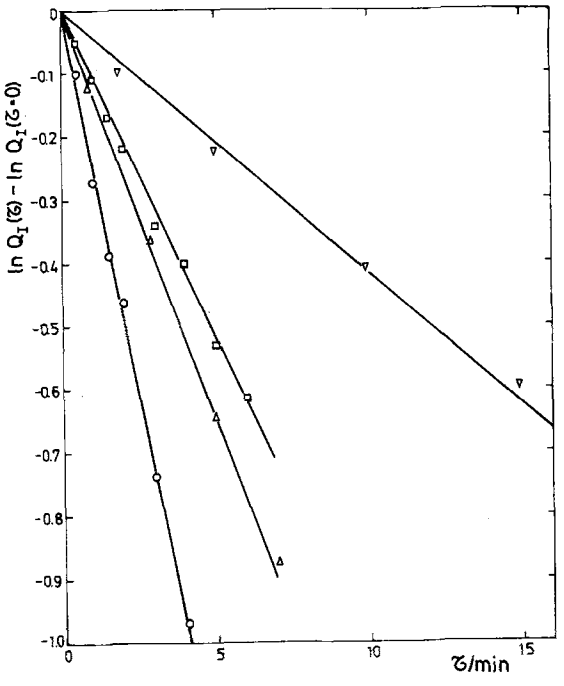


Fig. 9. First order plot for $Q_I$. (▽) $T = 0°$ C, (□) $T = 25°$ C, (△) $T = 50°$ C, and (○) $T = 75°$ C.

$$\ln \frac{Q_I(\tau = 0)}{Q_I(\tau)} = k_1 \tau = \ln \frac{Q_{II}(\tau)}{Q_{II}(\tau = 0)} \qquad (6)$$

$Q_I(\tau = 0)$ denotes the initial charge value of the reactant in Reaction 3. The average values of $k_1$ derived by plotting Equation 6 are shown in Figs. 9 and 10.

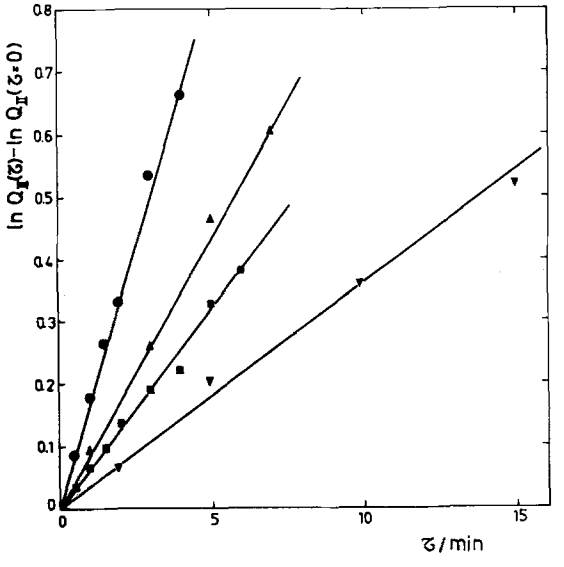


Fig. 10. First order plot for $Q_{II}$. (▼) $T = 0°$ C, (■) $T = 25°$ C, (▲) $T = 50°$ C and (●) $T = 75°$ C.

The same procedure is employed to calculate $k_2$, the formal rate constant for the second chemical process, assisted by the potentiodynamic ageing, namely:

$$[\mathrm{NiOOH}]_u \xrightarrow{k_2} [\mathrm{NiOOH}]_s \qquad (7)$$

In this case, however the interpretation becomes more involved since [6]

$$Q_{T,c} = Q_{III} + Q_{IV} + Q_s$$

where $Q_{T,c}$ is the total cathodic charge at any splitting, $Q_{III}$ is the charge of the cathodic current peak located at more positive potentials and $Q_{IV}$ is the charge of the cathodic current peak located at more negative potentials. $Q_{III}$ and $Q_{IV}$ are the charges of the cathodic current peaks whose relative contributions are particularly influenced by the potentiodynamic ageing. $Q_s$ is the charge of the third cathodic current peak whose potential depends on the temperature and is hardly affected by the potentiodynamic ageing. Consequently for the evaluation of $k_2$, $Q_{T,c}$ is taken as the sum $Q_{III} + Q_{IV}$. The charge $Q_{III}$ can be associated with the reaction

$$\mathrm{H^+ + e + [Ni(OOH)]}_u \rightleftharpoons [\mathrm{Ni(OH)_2}]_s \qquad (8)$$

and $Q_{IV}$, is the charge pertaining to the reaction:

$$\mathrm{H^+ + e + [NiOOH]}_s \rightleftharpoons [\mathrm{Ni(OH)_2}]_u \qquad (9)$$

Analogously to the previous case, $-\mathrm{d}Q_{III}/\mathrm{d}\tau = \mathrm{d}Q_{IV}/\mathrm{d}\tau$, and assuming a first order rate process, one obtains:

$$k_2 \tau = \ln \frac{Q_{III}(\tau = 0)}{Q_{III}(\tau)}. \qquad (10)$$

The values of $k_2$ are obtained from the plot shown in Fig. 11. The corresponding half-life times, $(t_i)_{1/2} = 0.693/k_i$, of Reactions 2 and 7 are also included in Figs. 12 and 13.

In the preceding analysis, the time related to Reaction 2 and 7 has been taken as equal to the time $\tau$ potentiodynamic ageing. This approximation is justified on the basis that the splitting of the current peaks obtained through the potentiodynamic ageing is similar to the splitting obtained from either the open circuit ageing or the potentiostatic ageing [7]. The average values of $k_1$

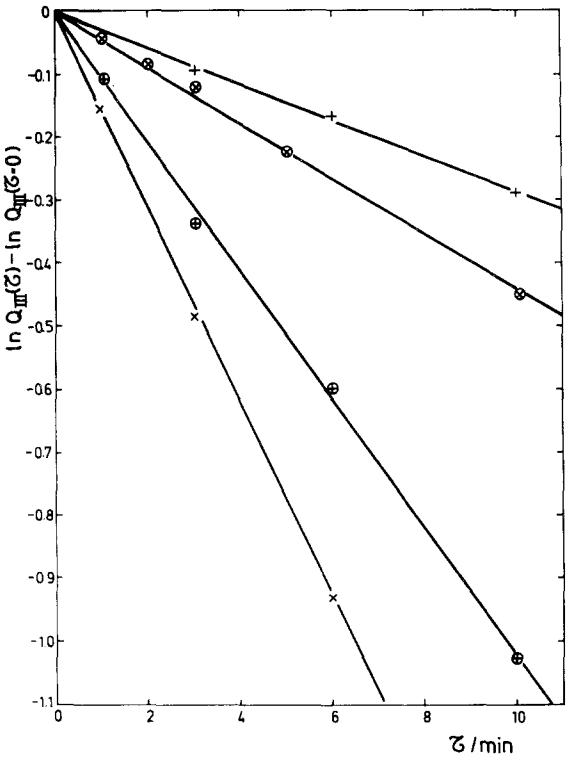


Fig. 11. First order plot for $Q_{III}$. (+) $T = 0°$ C, (⊗) $T = 25°$ C, (⊕) $T = 50°$ C, and (×) $T = 75°$ C.

and $k_2$ are independent of the frequency range and switching potentials related to the potentiodynamic ageing. The correction of $\tau$ due to the time spent in recording the $E/I$ display following the intermediate potential perturbation is negligible.

Both rate constants, $k_1$ and $k_2$, fit Arrhenius plots (Figs. 12 and 13). The experimental activation energy for Reaction 2 is $\Delta E_2^* = 4.2 \pm 0.2$ kcal mol$^{-1}$ and that of Reaction 7 is $\Delta E_7^* = 3.4 \pm 0.2$ kcal mol$^{-1}$.

### 4.3. *Possible structural characteristics related to the electrochemical reactions*

The complex reactions in the solid state phases related to the nickel hydroxide electrode were studied by X-ray [14, 16], infra-red [17], and *in situ* ellipsometric measurements [18–20] and interpreted on the basis of two forms of nickel hydroxide, namely the α-Ni(OH)$_2$ and the β-Ni(OH)$_2$ forms. Likewise, the γ-NiOOH and β-NiOOH forms of the Ni(III) species are also reported in the literature [14, 20–27]. The relative amount of each of these species depends on the charging and discharging conditions of the nickel hydroxide electrode [20, 22, 26–28] and on the concentration and composition of the electrolyte [27, 28].

The formation of β-NiOOH from the usual brucite modification β-Ni(OH)$_2$ implies no change in the main structural features [23], although this depends on the rate of electrooxidation [29–31]. The loosely hydrated α-Ni(OH)$_2$ species undergo electrochemical oxidation to γ-NiOOH, a species which retains its octahedral group of oxygen atoms with interlaminar material consisting of disordered water molecules and small quantities of alkali metal ions. However, the cell dimensions of γ-NiOOH vary greatly as the oxidation value of the nickel changes. Although these changes

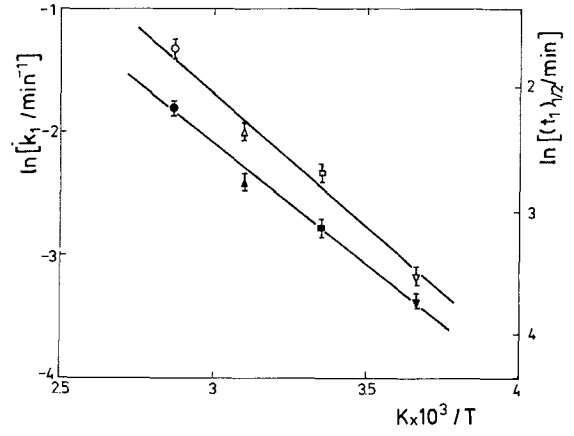


Fig. 12. Arrhenius plots for $k_1$ derived from data of Figs. 9 and 10.

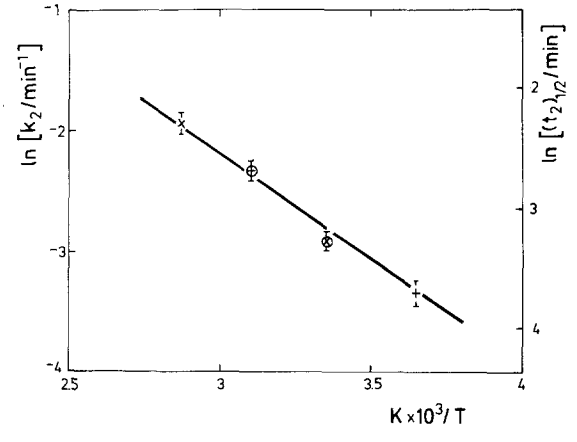


Fig. 13. Arrhenius plot for $k_2$ derived from data of Fig. 11.

cannot be expressed by simple stoichiometric ratios, they indicate the possibility of the NiOOH species having a larger number of structurally defined surface species. This can be associated with the more composite $E/I$ display for the electroreduction of the NiOOH species. The cathodic current peak located at more negative potentials is associated with the most stable NiOOH-species which may be related to the highly oxidized $\gamma_1$-nickel hydroxide [32] which appears to be formed as the innermost hydroxide layer in contact with the metal surface although the charge is lower than that expected for a full monolayer. The structures of these species vary in their water content [33] and with the possibility of cation incorporation into the lattice [34].

An identification of the $u$- and the $s$-species as some of the compounds referred to above may be attempted through the evaluation of the thermal data. If the $\alpha$-$Ni(OH)_2$ and $\beta$-$Ni(OH)_2$ are tentatively assigned to the $u$- and $s$-$Ni(OH)_2$ species respectively, Reactions 3 and 4 coincide with those postulated earlier by several authors when the NiOOH-species in Reaction 3 is $\gamma$-NiOOH and in Reaction 4 is $\beta$-NiOOH respectively [4, 7, 14, 24, 26, 27]. The kinetic analysis of these reactions was mainly directed towards the contribution of the crystal growth of the different species [24, 35] and to the participation of the diffusion of the mobile species in the electrode reaction [36–40]. In both cases the contributions of the chemical Reactions 2 and 7, although considered, were defined. But the main conclusion was, however, that there was no evidence that an appreciable charge transfer overpotential is associated with Reactions 3 and 4. On the basis of these conclusions it seems reasonable to admit that Reactions 3 and 4 are in quasi-equilibrium, so that the corresponding standard free energy difference can be estimated from the difference of the corresponding anodic current peak potentials:

$$\Delta G_4^0 - \Delta G_3^0 \approx -F(E_{p,II} - E_{p,I}) = -1.3 \pm 0.1 \text{ kcal mol}^{-1} \quad (11)$$

On the other hand, if in a more general way one considers that a process such as [29, 41]:

$$Ni(OH)_2 \text{ (disordered)} \rightarrow Ni(OH)_2 \text{ (ordered)} \quad (12)$$

is spontaneous at room temperature, then the corresponding $\Delta G_{12}$ value is negative. The upper limiting $\Delta G_{12}$ value as estimated from the solubility products of the $\alpha$-$Ni(OH)_2$ and $\beta$-$Ni(OH)_2$ [42–45] is $\Delta G_{12} = -3.4 \text{ kcal mol}^{-1}$. In this case it has been presumed that the $\alpha$-form is the most active one [14]. Reaction 12 should be associated with the transformation of the unstable into the stable $Ni(OH)_2$ species in the reaction pattern already described. Consequently, from the data of Reactions 3 and 4 assumed in equilibrium, the estimated standard free energy change of Reaction 7 results: $\Delta G_7 = -4.7 \text{ kcal mol}^{-1}$. The thermodynamic prediction for the spontaneous reaction is in this case, in agreement with the experimental findings [14, 26, 27].

## Acknowledgements

INIFTA is sponsored by the Consejo Nacional de Investigaciones Científicas y Técnicas, the Universidad Nacional de La Plata and the Comisión de Investigaciones Científicas (Provincia de Buenos Aires). This work was partially supported by the Regional Program for the Scientific and Technological Development of the Organization of American States and SENID (Navy Research and Development Service of Argentina).

H.G.M. thanks the leave of absence and financial assistance from the Universidad Católica de Valparaíso, Chile.

## References

[1] J. L. Weininger and M. W. Breiter, *J. Electrochem. Soc.* **110** (1963) 484.
[2] *Idem, ibid* **111** (1964) 707.
[3] Yu. N. Chernykh and A. A. Yakovleva. *Elektrokhimiya* **6** (1970) 1671.
[4] D. M. MacArthur, *J. Electrochem. Soc.* **117** (1970) 422.
[5] R. S. Schrebler Guzmán, J. R. Vilche and A. J. Arvía, *J. Appl. Electrochem.* **8** (1978) 67.
[6] *Idem, J. Electrochem. Soc.* **125** (1978) 1578.
[7] *Idem, J. Appl. Electrochem.* **9**, (1979) 183.
[8] *Idem, ibid* **9** (1979) 321.
[9] A. J. Arvía, *Israel J. Chem.*, in press.
[10] J. R. Vilche and A. J. Arvía, *Proceedings 4th International Symposium on Passivity*, Virginia, 1977 (edited by R. P. Frankenthal and J. Kruger,) p. 861.
[11] R. S. Schrebler Guzmán, J. R. Vilche and A. J. Arvía, *Corros. Sci* **18** (1978) 765.
[12] G. Milazzo and S. Caroli, 'Tables of Standard

Electrode Potentials', John Wiley, New York (1978).
[13] G. Kortüm, 'Kolorimetrie, Photometrie und Spektrometrie', 4.Aufl., Berlin (1962).
[14] H. Bode, K. Dehmelt and J. Witte, *Electrochim. Acta* **11** (1966) 1079.
[15] E. Jost and F. Rufenacht, *J. Electrochem. Soc.* **113** (1966) 97.
[16] S. U. Falk, *J. Electrochem. Soc.* **107** (1960) 661.
[17] F. P. Kober, *ibid* **114** (1967) 215.
[18] Y. N. Chernykh and A. A. Yakovleva, *Elektrokhimiya* 7 (1971) 530.
[19] *Idem*, *ibid* 7 (1971) 533.
[20] M. A. Hopper and J. L. Ord, *J. Electrochem. Soc.* **120** (1973) 183.
[21] M. A. Aia, *ibid* **113** (1966) 1045.
[22] H. Bode, K. Dehmelt and J. Witte, *Z. anorg. allg. Chemie* **366** (1969) 1.
[23] R. S. McEwen, *J. Phys. Chem.* **75**(1971) 1782.
[24] G. W. D. Briggs and M. Fleischmann, *Trans. Faraday Soc.* **67**, (1971) 2397.
[25] J. L. Ord, *Proceedings 4th International Symposium on Passivity*, Virginia 1977, (edited by R. P. Frankenthal and J. Kruger) p. 273.
[26] J. L. Ord, *Surface Sci.* **56** (1976) 413.
[27] N. Yu. Uflyand, A. M. Novakovskii and S. A. Rozentsveig, *Elektrokhimiya* 3 (1967) 537.
[28] O. G. Malandin, P. D. Lukovtsev and T. S. Tikhonova, *ibid* 7 (1971) 655.
[29] G. W. D. Briggs and W. F. K. Wynne-Jones, *Electrochim. Acta* 7 (1962) 241.
[30] G. W. D. Briggs, G. W. Stott and W. F. K. Wynne-Jones, *ibid* 7 (1962) 249.
[31] S. Le Bihan, J. Guenot and M. Figlarz, *CR Acad. Sci.* **270C** (1970) 2131.
[32] H. Bartl, H. Bode, G. Sterr and J. Witte, *Electrochim. Acta.* **16** (1971) 615.
[33] W. Dennstedt and W. Löser, *ibid* **16** (1971) 429.
[34] P. L. Bourgault and B. E. Conway, *Canad. J. Chem.* **38** (1960) 1557.
[35] G. W. D. Briggs and M. Fleischmann, *Trans. Faraday Soc.* **62** (1966) 3217.
[36] F. P. Kober, *J. Electrochem. Soc.* **112** (1965) 1064.
[37] P. D. Lukovtsev, *Elektrokhimiya* 4 (1968) 379.
[38] H. Ewe and A. Kalberlah, *Electrochim. Acta* **15** (1970) 1185.
[39] V. A. Volynskii and Yu. N. Chernykh, *Elek Elektrokhimiya* **12** (1976) 979.
[40] *Idem*, *ibid* **13** (1977) 1070.
[41] G. Feuillade and R. Jacoud, *Electrochim. Acta* **14** (1969) 1297.
[42] W. Feitknecht and P. Schindler, 'Löslichkeitskonstanten', Butterworths, London (1963).
[43] S. Okada, T. Shiraishi and K. Watanabe, *J. Soc. Chem. Ind. Japan* **51** (1948) 129.
[44] *Idem*, *ibid* **52** (1949) 37.
[45] *Idem*, *ibid* 53 (1950) 5.
[46] D. D. Macdonald, 'Modern Aspects of Electrochemistry', Vol. 11 (edited by B. E. Conway and J. O'M. Bockris) Plenum Press, New York, (1975) p. 141.
[47] G. W. D. Briggs, 'Electrochemistry', Vol. 4, Specialist Periodical Reports, The Chemical Society, London (1974).